Praise Worthy Prize

International Review of Chemical Engineering (I.RE.CH.E.), Vol. 5, N. 1
ISSN 2035-1755 *January 2013*

Hybrid First-Principle/Neural Network Correlations for Thermoelectric Transport Coefficients in Gold-Silver Solutions from Bulk to Nanometer Scale

Faïçal Larachi[1,2], Caroline Olsen[1]

Abstract – *State of art estimation methods were revisited to build hybrid first-principle/artificial neural network correlations to capture the impact of solute concentration, specimen sizes down to nanometer scale, and electron and phonon temperatures in (non)equilibrium for the electric and thermal transport coefficients in gold-silver mixtures at temperatures above the metals Debye temperatures. Deviations with respect to Matthiessen's additivity rule of both electric and electronic thermal transport coefficients were approximated by means of two neural network correlations as a function of silver atom fraction and temperature. The hybrid approach was confronted and validated against a large repository of data recommended for gold-silver transport properties encompassing pure metals and the full binary-solution composition range. Sensitivity of electric and thermal conductivities in gold-silver mixtures to electron and phonon temperatures, nanoparticle sizes and silver contamination was also discussed in the developed frame. The developed correlations will be useful for estimation of transport properties in areas as diverse as catalysis, electrochemical dissolution and gold nanomaterial synthesis.*

Keywords: *Gold-Silver Mixture Electric and Thermal Conductivities; Electron and Phonon Scattering, Relaxation Time; Correlation; Metal Nanoparticle; Electron-Phonon Non-Equilibrium*

Nomenclature

a	Lattice constant, m or Å
A	Parameter in N-processes equation for relaxation time, K^{-3}
A_{ee}	Parameter in (electron-electron) electric resistivity contribution, Ω m/K^2
A_{ep}	Parameter in high-temperature (electron-phonon) electric resistivity approximation, Ω m
b	Parameter in U-processes for relaxation time
c	Atom fraction of impurity in crystal lattice
d	Particle diameter, m
D_{pe}	Phonon-electron Makinson parameter, m^{-1}
e	Electron charge, 1.6022 E-19 C
E_F	Fermi energy, J
F	Function in relaxation time for electron scattering on lattice impurity, $F(y) = 2y^{-2}(\ln(1+y)-y(1+y)^{-1})$-
G	Parameter in high-temperature lattice (phonon-electron) thermal conductivity, W/m/K
H	ANN hidden-layer normalized variable
k	Phonon wave number, m^{-1}
k_B	Boltzmann constant, 1.3806 E-23 J/K
k_F	Fermi wave number, m^{-1}
k_{TF}	Thomas-Fermi screening parameter, m^{-1}
h	Planck constant, 6.6261 E-34 J s
$\hbar$	$h/(2\pi)$, reduced Planck (Dirac) constant, 1.0546 E-34 J s
L_0	Standard Lorentz number, $\pi^2/3\ (k_B/e)^2$ = 2.44 E-8 V^2/K^2
m_a	Average mass of a single atom in a solid or mass of host atom, kg
m_e	Free electron mass, kg
m_I	Mass of impurity atom in a solid, kg
n_e	Number density of conduction electrons in a metal at equilibrium, m^{-3}
T	Absolute temperature, K
U	ANN input layer normalized variable
v	Average speed of sound, m/s
v_F	Electron velocity at Fermi surface, m/s
V_0	Atomic volume, $a^3/4$ m^3 per atom
x	Phonon energy normalized with respect to thermal energy, $x = \hbar\omega/(k_B T)$
y	Dummy variable in function F, $y = 4k_F^2 / k_{TF}^2$
z	Nominal valence, z = 1 for monovalent metal
z_I	Nominal valence of (static) impurity atoms
α	Fitting parameters in ANN Δ function
β	Fitting coeff of residual electric conductivity
Γ	Sommerfeld parameter, 71.4 J/m^3/K for Au
γ	Grüneisen constant, 3.16 for Au at 0.1 MPa
δ	Thermal resistivity deviation from Matthiessen's rule, K m/W
Δ	Electric resistivity deviation from Matthiessen's rule, Ω m

Manuscript received and revised December 2012, accepted January 2013

θ_D Debye temperature for phonons
κ Overall thermal conductivity, W/m/K
κ_a Lattice thermal conductivity, W/m/K
κ_e Electronic thermal conductivity, W/m/K
κ_{eB} (Electron-boundary) electronic thermal conductivity, W/m/K
κ_{ee} (Electron-electron) electronic thermal conductivity, W/m/K
κ_{eI} (Electron-impurity) electronic thermal conductivity, W/m/K
κ_{ep} (Electron-phonon) electronic thermal conductivity, W/m/K
κ_{pe} (Phonon-electron) lattice thermal conductivity, W/m/K
λ Phonon wavelength, m
σ_e Overall electric conductivity, Ω^{-1} m^{-1}
σ_{eB} (Electron-boundary) contribution to electric conductivity, Ω^{-1} m^{-1}
σ_{ee} (Electron-electron) contribution to electric conductivity, Ω^{-1} m^{-1}
σ_{eI} (Electron-impurity) contribution to electric conductivity, Ω^{-1} m^{-1}
σ_{ep} (Electron-phonon) contribution to electric conductivity, Ω^{-1} m^{-1}
$\tau_{eB(\kappa)}$ Electron-boundary scattering thermal relaxation time, s
$\tau_{eB(\sigma)}$ Electron-boundary electric scattering relaxation time, s
$\tau_{ee(\kappa)}$ Thermal relaxation time for electron scattering on electron, s
$\tau_{ee(\sigma)}$ Electric relaxation time for electron scattering on an electron, s
$\tau_{eI(\kappa)}$ Thermal relaxation time for electron scattering on impurity, s
$\tau_{eI(\sigma)}$ Electric relaxation time for electron scattering on impurity, s
$\tau_{ep(\kappa)}$ Thermal relaxation time for electron scattering on a phonon, s
$\tau_{ep(\sigma)}$ Electric relaxation time for electron scattering on a phonon, s
τ_N Relaxation time for phonon-phonon normal processes, s
τ_{pB} Phonon relaxation time for crystal particle boundary scattering, s
τ_{pe} Relaxation time for phonon scattering on an electron, s
τ_{pI} Relaxation time of point-defect (Rayleigh) scattering of phonon from isolated impurity, s
τ_r Overall phonon relaxation time for resistive processes, s
τ_U Umklapp relaxation time for phonon-phonon scattering, s
ω Phonon angular frequency, rad/s

Sub/superscripts

a Relative to dominant metallic atom in lattice or relative to acoustic phonon
calc. Calculated
e Relative to electron
exp Experimental
I Impurity
min Lower-range value
max Upper-range value

I. Introduction

Mine production is by far the main supply of gold driven by a steadily climbing world demand for this metal to respond to growing needs both in mature as well as in emerging industrial sectors. Native gold grains dealt with in mining operations contain up to 99.8% weight percent Au but contents as low as 85% are not uncommon with silver being the main solute impurity [1]. The most common non-chemical recovery processes of native gold consist of gravity concentration and flotation while gold leaching is the chemical process *par excellence* to cope with the tailings refractoriness by dissolving gold through oxidative-complexation cyanidation. In many technological areas, knowledge of the electric and thermal transport properties of such naturally occurring gold-alloy systems is a crucial component for the control and prediction of the material's physical and chemical response under thermal gradient, electric field or laser irradiance constraints. Electrochemical anodic dissolution of gold is known to be very sensitive to the occurrence of silver traces thus impacting the rate of gold dissolution in cyanidation plants [2]. In catalytic reactions, nano-sized gold is increasingly stared at as a potential substitute to replace costly platinum group metals in automotive catalytic converters [3], beside a plethora of catalytic applications of gold in pollution mitigation and chemical conversion [4], [5]. Likewise, numerous emerging micro-fabrication technologies of gold nanostructures such as those based on pulsed-laser deposition of thin films or on chemical synthesis routes are witnessing an effervescent activity both in academia and industry [6]-[9]. Considering the rejuvenated interest in conventional precious metal-based processes and the incipient catalysis and nanotechnology areas ogling gold, we propose to revisit in this contribution the state of art estimation methods for the prediction of electric and thermal transport properties of gold-silver alloys. Specifically, we will assess the merit of a simple and original approach based on combining first-principle transport phenomena of electrons and acoustic phonons with artificial neural network correlations to capture the influence of solute concentration, specimen size, and charge/heat carrier temperatures in (non)equilibrium for the electric and thermal transport coefficients in gold-silver alloys.

II. Theory

II.1. Electric and Electronic Thermal Conductivity

Scattering of electrons in metal solutions subject to

external electric fields and thermal gradients is responsible for the finite electric and thermal conductivities, the origin of which stems from electron interactions with solute (impurity) atoms, lattice phonons and Fermi near-edge (conduction) electrons. Such events are gathered in *intrinsic* electric ($\sigma_{ep}+\sigma_{ee}$) and electronic thermal ($\kappa_{ep}+\kappa_{ee}$) conductivities that arise due to inelastic/elastic electron-phonon and electron-electron scattering, and in *residual* electric (σ_{el}) and electronic thermal (κ_{el}) conductivities due to elastic electron-impurity scattering [10],[11].

Furthermore, depending on whether momentum conservation is violated or preserved, and whereby collisions correspondingly imply nonzero or zero values of the reciprocal lattice vector, electron-phonon and electron-electron interactions either lead to a reduction of metal conductivities *via* umklapp scattering or leave transport properties unimpeded *via* normal scattering. At high temperatures, *i.e.*, above the metal Debye temperature, electron-phonon umklapp processes outweigh normal processes owing to a larger reservoir of phonons excited close to the Debye wave number. Such large wave-number phonons at high temperature also induce directional changes of electrons *via* elastic large-angle scattering. On the other hand, umklapp electron-electron scattering is important in the case of noble metals as they exhibit among the highest effectiveness parameter values [11] whereas normal electron-electron scattering is inelastic and contributes to thermal conductivity [10].

In addition, when sample sizes approach electrons' mean free path such as for nanosized metallic particles, boundary scattering markedly reduces transport properties *via* electron-boundary electric (σ_{eB}) and thermal (κ_{eB}) conductivities. Finally, for binary solutions of ordinary monovalent metals, such as $Au_{1-c}Ag_c$ mixtures, the intrinsic electric and electronic thermal conductivities are typically computed from barycentric approximations of virtual alloy crystals using atom-fraction weighted properties of the pure host and solute elements [12].

In the context of mutually independent scattering phenomena, one often has recourse to Matthiessen's rule for additive aggregation of above transport contributions. However, this rule breaks down when electron scattering by solute and by phonons are not independent of each other as may be the case in alloys [13]. Electric, $\Delta(c,T)$, and thermal, $\delta(c,T)$, deviation functions that depend on solute atom fraction, c, and temperature, T, must therefore be introduced to account for the gap between actual intrinsic transport properties and those computed for a virtual alloy crystal assuming Matthiessen's rule.

The phenomenological relationship of thermal conductivity arising from kinetic theory enables to relate the various electronic thermal conductivity components to their corresponding thermal relaxation times as $\kappa_{ej} = 1/3\Gamma T_e v_F^2 \tau_{j(\kappa)}$ (Readers are invited to consult the detailed nomenclature section available in the supporting information). Likewise, from the linearized Boltzmann equation and its relaxation time approximation, it is possible to establish a generic dependence between electric conductivity due to electrons that travel over the Fermi surface at the Fermi velocity and electric relaxation time as $\sigma_{ej}=n_e e^2 \tau_{j(\sigma)}/m_e$.

Finally, electric and electronic thermal conductivities pinned to each mechanism are often paired *via* Wiedemann-Franz type of laws and electron-gas temperature, T_e.

Considering that the lattice (or phonon) temperature, T_a, is the reservoir temperature and assuming the case of electron-lattice non-equilibrium, the electric and electronic thermal conductivity and relaxation time contributions by electron-phonon scattering in the high-temperature limit are given by [11]:

$$\frac{1}{\sigma_{ep}} = \frac{A_{ep}}{4}\frac{T_a}{\theta_D} \tag{1}$$

$$\frac{1}{\tau_{ep(\sigma)}} = \frac{n_e e^2}{m_e}\frac{A_{ep}}{4}\frac{T_a}{\theta_D} \tag{2}$$

$$\frac{1}{\kappa_{ep}} = \frac{A_{ep}}{4L_0 T_e}\frac{T_a}{\theta_D}\left(1+0.1577\left(\frac{\theta_D}{T_a}\right)^2\right) \tag{3}$$

$$\frac{1}{\tau_{ep(\kappa)}} = \frac{A_{ep}\Gamma v_F^2}{12L_0}\frac{T_a}{\theta_D}\left(1+0.1577\left(\frac{\theta_D}{T_a}\right)^2\right) \tag{4}$$

Eq. (1) is the high-temperature limit of the Bloch-Grüneisen relation due to disturbance of crystal periodicity by the vibrating lattice ions [11]. The thermal and electric relaxation times (Eqs. (2),(4)) differ by a $1/T_a^2$ term in $\tau_{ep(\kappa)}$ contributed amongst others by inelastic small-angle scattering. In the limit of $T_a >> \theta_D$, Eq. (4) formally retrieves the electron-phonon function proposed by Ivanov and Zhigilei [14] and others [8],[15],[16] but the one proposed here is more general as it also includes thermal scattering terms beside the elastic large-angle scattering of electrons.

The electron-electron contribution to electric conductivity and electronic thermal conductivity reflects, for the former, in Fermi-liquid T^2 dependence, and for the latter, in an extension consistent with the Wiedemann-Franz law [11]. Expressions for the corresponding relaxation times are also derived:

$$\frac{1}{\sigma_{ee}} = A_{ee}T_e^2 \tag{5}$$

$$\frac{1}{\tau_{ee(\sigma)}} = \frac{n_e e^2}{m_e}A_{ee}T_e^2 \tag{6}$$

$$\frac{1}{\kappa_{ee}} = \frac{A_{ee}}{L_0} T_e \tag{7}$$

$$\frac{1}{\tau_{ee(\kappa)}} = \frac{A_{ee}}{3L_0} \Gamma v_F^2 T_e^2 \tag{8}$$

The electron-impurity scattering is typically formalized by means of the Born approximation. Since this formulation is known to overestimate scattering by impurities [11], we modified its expression to become consistent with the solute concentration structure of the Nordheim's rule for the residual electric conductivity in binary noble-metal solid-solution alloys [13].

As will be discussed later, a proportionality constant, β, was thus fitted using residual electric conductivity data for the Au-Ag binary alloy systems below 4 K [13]. Expressions for electric residual conductivity and its corresponding relaxation time are thus established:

$$\frac{1}{\sigma_{eI}} = \frac{2\pi}{3} \frac{m_e}{n_e e^2} \beta \frac{E_F}{\hbar} z_I^2 F(y) c(1-c) \tag{9}$$

$$\frac{1}{\tau_{eI(\sigma)}} = \frac{2\pi}{3} \beta \frac{E_F}{\hbar} z_I^2 F(y) c(1-c) \tag{10}$$

Electrons scatter elastically on static imperfections thus making the Wiedemann-Franz law applicable for inferring the electronic thermal conductivity, κ_{eI}, from its sibling electric counterpart, σ_{eI}, as well as the associated thermal relaxation time:

$$\frac{1}{\kappa_{eI}} = \frac{2\pi}{3} \beta \frac{m_e}{n_e e^2} \frac{E_F}{\hbar L_0 T_e} z_I^2 F(y) c(1-c) \tag{11}$$

$$\frac{1}{\tau_{eI(\kappa)}} = \frac{2\pi}{9} \beta \frac{m_e}{n_e e^2} \frac{E_F}{\hbar L_0} z_I^2 F(y) c(1-c) \Gamma v_F^2 \tag{12}$$

We will make the same assumption that boundary scattering is reminiscent of scattering on static lattice imperfections as the relaxation time for this mechanism is also independent of temperature [15].

Therefore, we will assume that the electron-boundary contribution to electric and electron thermal conductivities also obeys a Wiedemann-Franz type law:

$$\kappa_{eB} = 3^{-1} \Gamma T_e d v_F \tag{13}$$

$$\frac{1}{\tau_{eB(\kappa)}} = \frac{v_F}{d} \tag{14}$$

$$\sigma_{eB} = \frac{\Gamma d v_F}{3L_0} \tag{15}$$

$$\frac{1}{\tau_{eB(\sigma)}} = \frac{3L_0}{\Gamma d v_F} \frac{n_e e^2}{m_e} \tag{16}$$

II.2. Thermal Lattice Conductivity

Although heat conduction by lattice waves is often marginal in pure non-transition metals in comparison with electron-mediated heat conduction, its contribution in alloy systems may not be totally ignored [12].

Therefore, to keep our approach comprehensive, we have chosen to describe thermal conduction by lattice vibrations in metal solutions by means of the exhaustive Callaway's framework [17], [18].

Hence, use is made of the Debye phonon dispersion relation to account for both normal and umklapp phonon-phonon scattering together with the other coexisting phonon-electron, phonon-impurity, and phonon-boundary collisional events which contribute to resistive lattice heat transport.

In the Debye model, all branches in the acoustic phonon vibrational spectrum are replaced by 3 (1 longitudinal and 2 transverse) branches with same linear *isotropic* dispersion law.

Assuming mutual independence between resistive processes, the Matthiessen's additivity rule, akin to the earlier electronic analog, can be resorted to for clustering those events' associated collision frequencies. The higher-frequency phonons whose phonon-phonon collisions bring about offspring phonons to lie outside the first Brillouin zone (umklapp scattering) are accounted for *via* Matthiessen's rule. Unlike these phonons, the ones pertaining to the lower-frequency end of the density-of-states require special treatment as their phonon-phonon interactions induce zero reciprocal lattice vectors (normal scattering) and do not give rise directly to thermal resistance.

Their corresponding collision frequency cannot *per se* be aggregated *via* Matthiessen's rule, which is remedied by recourse to Callaway's approach.

Their indirect effect on thermal conduction translates *via* energy exchanges from low- to high-frequency phonon modes, such as in the case of strongly frequency-sensitive phonon-impurity and phonon-phonon umklapp scattering mechanisms.

The phonon energy is often expressed as a fraction of the lattice thermal energy as follows for the prevailing lattice temperature, T_a:

$$\omega = vk = v\frac{2\pi}{\lambda} = \frac{k_B T_a}{\hbar} x \tag{17}$$

Assuming that the average speed of sound in the solid solution as given by the isotropic linear dispersion Debye model is valid [19], one obtains:

$$v = \frac{k_B \theta_D a}{h} \left(\frac{\pi}{3} \right)^{1/3} \tag{18}$$

where the lattice parameter, a, of the gold-silver solution is calculated using the Au-Ag alloy density correlation developed by Kraut and Stern [20]. The relaxation time, τ_U, for phonon scattering on phonons (umklapp processes) is expressed as [21]:

$$\frac{1}{\tau_U} = \frac{\hbar\gamma^2}{m_a v^2}\frac{T_a}{\theta_D} e^{-\frac{\theta_D}{bT_a}} \omega^2 = \frac{k_B^2\gamma^2 T_a^3}{\hbar m_a v^2 \theta_D} e^{-\frac{\theta_D}{bT_a}} x^2 \quad (19)$$

Similarly, the relaxation time, τ_N, for phonon-phonon normal processes takes the form [18]:

$$\frac{1}{\tau_N} = \frac{A}{2\pi} T_a^3 \omega = \frac{A k_B}{2\pi\hbar} T_a^4 x \quad (20)$$

The relaxation time, τ_{pI}, stemming from phonon-impurity Rayleigh scattering in $Au_{1-c}Ag_c$ solid solution can be described using the following expression [22]:

$$\frac{1}{\tau_{pI}} = \frac{cV_0}{4\pi v^3}\left(1-\frac{m_I}{m_a}\right)^2 \omega^4 = \\ = \frac{cV_0}{4\pi v^3}\left(1-\frac{m_I}{m_a}\right)^2 \left(\frac{k_B T_a}{\hbar}\right)^4 x^4 \quad (21a)$$

The relaxation time, τ_{pe}, for phonon scattering on electrons is expressed from a relationship due to Makinson [23]:

$$\frac{1}{\tau_{pe}} = 2^{\frac{4}{3}} \frac{v\hbar D_{pe}}{k_B \theta_D}\omega = 2^{\frac{4}{3}} v D_{pe} \frac{T_a}{\theta_D} x \quad (21b)$$

Parameter D_{pe} was derived by Makinson [23] and was cast here in an expression that allows its calculation using G and A_{ep} estimated constants:

$$D_{pe} = \frac{3}{2\pi}\left(\frac{4\pi}{3}\right)^{1/3} \frac{\theta_D k_B^2}{\hbar G a^2} \quad (22)$$

Note that parameter G for phonon scattering on electrons as it appears in D_{pe} was estimated from the ratio of the high-temperature approximations of lattice (phonon-electron) and electronic (electron-phonon) thermal conductivities [11]:

$$\frac{\kappa_{pe}}{\kappa_{ep}} = \frac{GA_{ep}}{8L_0\theta_D} = \frac{1.03}{z} \quad (23)$$

For monovalent metals (z = 1, *i.e.*, one free electron per lattice ion) such as gold or silver, one obtains:

$$G = 8.24 L_0 \frac{\theta_D}{A_{ep}} \quad (24)$$

Similarly, parameter A_{ep} (Eqs. (1), (3)) appearing in the high-temperature approximation of (electron-phonon) electric conductivity contribution is obtained from fitting the high-temperature electric conductivity data from Ho et al. [13] as explained later.

Finally, assuming a totally diffuse phonon scattering at the surface of the sample, the phonon relaxation time, τ_{pB}, for crystal boundary scattering is given by [21]:

$$\tau_{pB}^{-1} = \frac{v}{d} \quad (25)$$

II.3. Overall Electric and Thermal Conductivities

By distinguishing between lattice and electron temperatures in the general case of electron-phonon non-equilibrium energy transfer conditions for the various scattering mechanisms outlined above, the following composition-temperature relationships for the overall electric (σ_e), and electronic (κ_e), lattice (κ_a) and total metal solution (κ) thermal conductivities are established (host metal = a, solute impurity = I) in the case of $Au_{1-c}Ag_c$ metal solutions:

$$\frac{1}{\sigma_e} = (1-c)\left(\frac{A_{ep,a}}{4}\frac{T_a}{\theta_{D,a}} + A_{ee,a}T_e^2\right) + \\ + c\left(\frac{A_{ep,I}}{4}\frac{T_a}{\theta_{D,I}} + A_{ee,I}T_e^2\right) + \\ + \frac{2\pi}{3}\beta\frac{m_e}{n_e e^2}\frac{E_F}{\hbar} z_I^2 F(y) c(1-c) + \\ + \frac{3L_0}{\Gamma_a v_{F,a} d} + \Delta \quad (26)$$

$$\frac{1}{\kappa_e} = (1-c)\left(\frac{A_{ep,a}}{4L_0\theta_{D,a}}\frac{T_a}{T_e}\left(1+0.1577\left(\frac{\theta_{D,a}}{T_a}\right)^2\right) + \right. \\ \left. + \frac{A_{ee,a}}{L_0}T_e\right) \\ + c\left(\frac{A_{ep,I}}{4L_0\theta_{D,I}}\frac{T_a}{T_e}\left(1+0.1577\left(\frac{\theta_{D,I}}{T_a}\right)^2\right) + \right. \\ \left. + \frac{A_{ee,I}}{L_0}T_e\right) + \\ + \frac{2\pi}{3}\beta\frac{m_e}{n_e e^2}\frac{E_F}{\hbar L_0 T_e} z_I^2 F(y) c(1-c) + \\ + \frac{3}{\Gamma_a T_e v_{F,a} d} + \delta \quad (27)$$

$$\kappa_a = \frac{k_B}{2\pi^2 v}\left(\frac{k_B T_a}{\hbar}\right)^3 \times \left(\int_0^{\frac{\theta_D}{T_a}} \left(\tau_r^{-1}+\tau_N^{-1}\right)^{-1} \frac{x^4 e^x dx}{\left(e^x-1\right)^2} + \frac{\left(\int_0^{\frac{\theta_D}{T_a}} \left(\tau_r^{-1}+\tau_N^{-1}\right)^{-1} \tau_N^{-1} \frac{x^4 e^x dx}{\left(e^x-1\right)^2} \right)^2}{\int_0^{\frac{\theta_D}{T_a}} \left(\tau_r+\tau_N\right)^{-1} \frac{x^4 e^x dx}{\left(e^x-1\right)^2}} \right) \quad (28)$$

$$\kappa = \kappa_e + \kappa_a \quad (29)$$

Eq. (28) is the Callaway's lattice thermal conductivity model [17] in which the overall resistive relaxation time, τ_r, has been defined by grouping altogether the resistive processes:

$$\tau_r^{-1} = \tau_U^{-1} + \tau_{pI}^{-1} + \tau_{pB}^{-1} + \tau_{pe}^{-1} \quad (30)$$

Note also that the integrals in Eq. (28) are computed using an estimate of the minimum value of the normalized phonon energy, x_{min}, in the integral lower-bound corresponding to a maximum phonon wavelength equal to the particle diameter:

$$x_{min} = \frac{2\pi\hbar v}{k_B T_a d} \quad (31)$$

III. Database and Computational Strategy

A database was first constituted using the recommended electric and thermal conductivity data published by CINDAS (Center for Information and Numerical Data Analysis and Synthesis) group.

The database consisted of 778 tabulated electric and thermal conductivities for pure gold, pure silver and mixtures thereof with a specific focus on the $T \geq \theta_D$ temperature range [12], [13], [24].

Due to their origin from macroscopic samples, the boundary scattering terms were neglected during model confrontation to the tabulated conductivity data. Also, electron-phonon equilibrium was assumed, $T_a = T_e = T$.

Parameters A_{ep} and A_{ee} depicting the intrinsic electric conductivity of *pure* metals contributed, respectively, by linear (Eq. (1)) and quadratic (Eq. (5)) temperature dependences were estimated using the tabulated electric conductivity values for pure gold (16 data) and pure silver (14 data) above their respective Debye temperatures as recommended by Ho et al. [13].

They were regressed using the high-temperature asymptotic expression $1/(T^2(\sigma_{ep}+\sigma_{ee})_j) = A_{ee,j} + A_{ep,j}/(4T\theta_{D,j})$, j = Au or Ag, where more weight is given to the high-temperature measurements in parameter estimation.

The predictive power of intrinsic electric conductivity parameters, A_{ep} and A_{ee}, to estimate, without further fitting, the total thermal conductivity recomposed using Eqs. (3),(7), (28) and (29) was assessed by using the total thermal conductivity data for the *pure* metals (26 data for Au and 26 data for Ag) recommended by Ho et al. [24]

The lattice contribution to thermal conductivity was computed with the aid of eqs. (17)-(25), (28).

The residual electric conductivity data, σ_{el}, were those recommended by Ho et al. [13] for Au-Ag solid solutions with silver atom fraction, c, sweeping the range [0.91 10^{-2} – 99.7 10^{-2}] and where a total of 25 data at temperatures below 4 K were culled to estimate parameter β from Eq. (9). Once parameters A_{ep}, A_{ee} and β were determined, a total of 371 electric conductivity data tabulated by Ho et al.[13] for the high-temperature ($T > \theta_D$) range of the Au-Ag alloy system were used to build from Eq. (26) the deviation function $\Delta(c,T)$ with respect to Matthiessen's rule of the electric conductivity in the binary gold-silver solutions. Similarly, a total of 300 total thermal conductivity data recommended by Ho et al. [12] for the high-temperature range for Au-Ag alloy systems were used to infer from eq. (27) the deviation function $\delta(c,T)$.

In this latter case, the lattice contribution to thermal conductivity was computed as for the pure metals with the aid of Eqs. (17)-(25),(28) and the total thermal conductivity was obtained using Eq. (29).

Finally, the residual values given by the deviation functions, Δ and δ, were regressed as a function of two input variables c and T using an artificial neural network (ANN) methodology with the help of NNFit software.[25]

These correlations are valid for the following composition and temperature conditions for Au_{1-c}-Ag_c solutions: [0.91 10^{-2} – 99.7 10^{-2}] for c, [200 – 1200] K for T in the case of Δ ([250 – 1200] K for T in the case of δ), [-4.75 10^{-9} –7.15 10^{-9}] Ω.m for Δ, and [-6. 15 10^{-4} – 5.09 10^{-4}] m.K/W for δ. The neural regression methodology is detailed in Larachi et al. [26] where the ANN parameters (weights) were fitted using training data sets consisting of 80% of each conductivity property database and the obtained ANN models were tested on generalization data sets with the remaining 20%.

Combination of the model (Eqs. (26)-(29)) with the Δ and δ neural network correlations is designated as a hybrid first-principle/artificial neural network model or simply hybrid model.

IV. Results and Discussion

IV.1. Pure Metal and Residual Conductivities

Fig. 1 illustrates the quality of fit of Eqs.(1),(5) *versus* intrinsic electric resistivity (reciprocal conductivity) data determined for pure gold and pure silver above their Debye temperatures. The respective standard deviations are 1.0% for Au and 1.1% for Ag.

The data fit for $T > \theta_D$ yields $A_{ep} = (452.4 \pm 2.3)\times10^{-10}$ Ω.m and $A_{ee} = (21.6 \pm 1.0)$ fΩ.m/K^2 for pure gold (θ_D = 165 K), and $A_{ep} = (445.3 \pm 2.9)\times10^{-10}$ Ω.m and $A_{ee} = (14.6 \pm 0.9)$ fΩ.m/K^2 for pure silver (θ_D = 225 K). The figure also illustrates predictability of pure Au and pure Ag total thermal conductivities using these parameters in Eqs.(3),(7).

The standard Lorentz-Sommerfeld number, L_0, was used in these equations and the lattice contribution to thermal conductivity was likewise accounted for as explained above. The thermal conductivity plots are shown for temperatures above the Debye temperatures for each metal with standard deviations of 1.1% for Au and 0.9% for Ag.

The fitted A_{ee} values for Au and Ag are an order of magnitude larger than those typically reported for the same metals [27] and might signify that the pure metal CINDAS data used here could be tainted with T^2 dependence from a different origin. Despite this state of affairs, restoration of thermal conductivity data without further fitting suffices to say that the parameters fitted on electrical conductivity data along with Wiedemann-Franz law bear some physical sense.

Prediction of the residual electric conductivity given by Eq. (9) can be judged from the quality of fit shown in Fig. 2. This figure compares low-temperature measured and fitted residual electric conductivity data with a standard deviation of 7.1% and parameter β was estimated to be $(155.8 \pm 1.2)\times10^{-3}$.

IV.2. Prediction of Binary Alloy Conductivities

By accounting for deviations in the overall electric resistivity and electronic thermal conductivity with respect to the Mathiessen's rule, and by expressing the ANN deviation functions Δ and δ in terms of variables *c* and *T*, a remarkable fit of the overall electric and total thermal conductivity data was achieved as shown in Figs. 3(a),(b) parity plots.

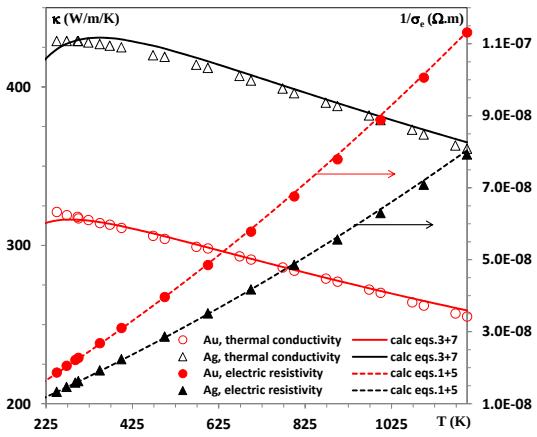

Fig. 1. Goodness of fit of eqs.1+5 to represent the temperature dependence of pure gold and pure silver electric resistivity and of Eqs. (3)-(7), aided with lattice thermal conductivity contribution, to predict the total metal thermal conductivity

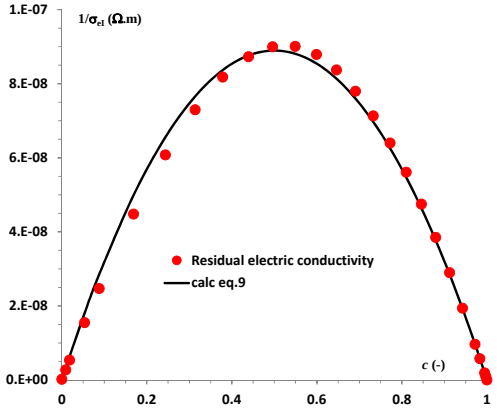

Fig. 2. Goodness of fit by eq.9 of the low-temperature residual electric resistivity as a function of silver concentration in $Au_{1-c}Ag_c$ alloy system

These figures illustrate validity of the hybrid model for the overall electric (σ_e) and total thermal (κ) conductivities in the case of $Au_{1-c}Ag_c$ metal solutions over the full compositional Au-Ag range in the elevated temperature domain. The standard deviations on relative residuals between tabulated and predicted data amounted to 1.6% and 0.7% (or equivalently the standard deviations on the absolute residuals were 1.3 10^{-9} Ω.m and 1.9 W/m/K), respectively, for $1/\sigma_e$ and κ. Most of the deviations out of 405 electric + 352 thermal coefficient data (Figs. 3(a),(b)) came from 15 high-temperature overall electric data (7 at 1200 K, 3 at 1100 K, 2 at 1000 K and 3 at 900 K) and 7 high-temperature thermal conductivity data (4 at 1100 K and 3 at 1000 K) for which lack of measurement accuracy might be invoked. The deviation functions, Δ and δ, were correlated using two artificial neural networks, each representing 2 input-layer neurons (*c*, *T*), 5 hidden-layer neurons and 1 output-layer neuron (Δ or δ) as summarized in Tables II and III. Adequacy of the developed hybrid model can be sensed also from the excellent fits illustrated in Figs. 3(c), (d) for some measured versus computed electric (Eq.(26)) and total thermal (Eqs. (27)-(29)) conductivities for gold-silver alloy compositions typical of native gold, *i.e.*, Ag atomic percent up to 25% [1]. Amelioration of model predictability while accounting for ANN-computed deviation functions, Δ and δ, can alternatively be assessed by comparing the proposed hybrid approach to the following simplified estimation approaches. In the first approach i), the electric and electronic thermal conductivity deviations were assumed to be interrelated using the Wiedemann-Franz law and the standard Lorentz-Sommerfeld number, L_0, *i.e.* $\delta = \Delta/(L_0 T)$ with Δ computed using Table I ANN correlation. In the second approach ii), it was assumed that both electric and electronic thermal conductivities can be described using solely Matthiessen's additivity rule, *i.e.*, Δ and δ are equal to zero. Table III summarizes the statistical figures of merit comparing the three approaches using the present transport coefficients database.

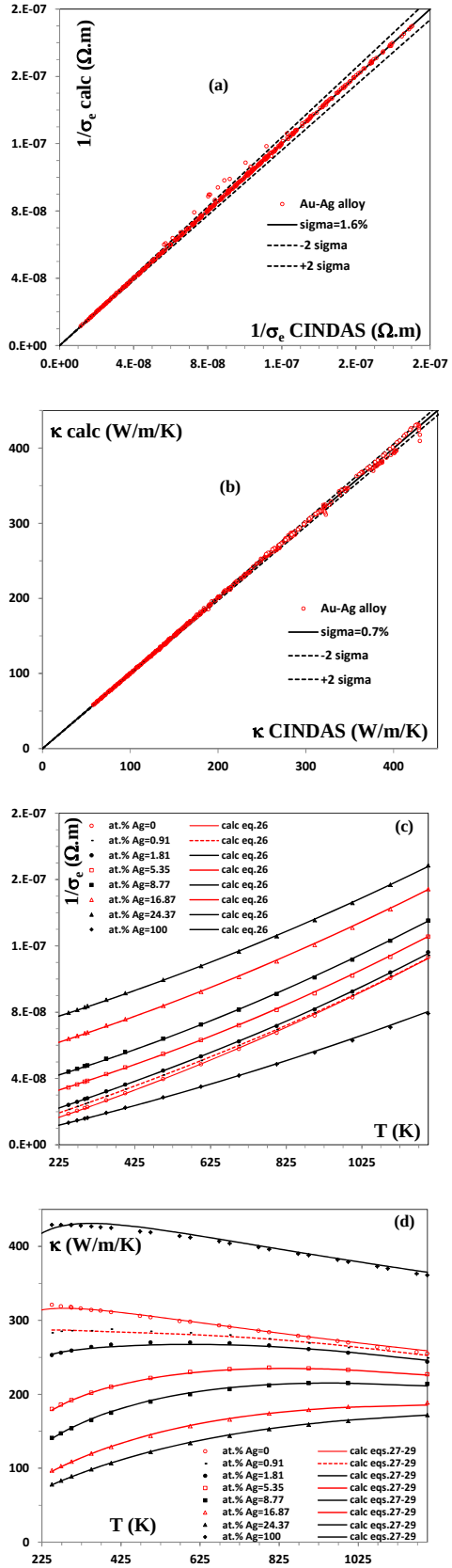

Figs. 3. Parity plot for the full compositional range of calculated from hybrid model (Eqs.(26)-(29), Tables I,II) versus (CINDAS) tabulated $Au_{1-c}Ag_c$ alloy (a) electric resistivity, (b) total thermal conductivity, and selected temperature-composition plots for electric resistivity (c) and total thermal conductivity (d) up to 25% silver content

Inclusion of ANN-computed electric deviation function and inference of thermal deviation function *via* a Wiedemann-Franz law and standard Lorentz-Sommerfeld number (approach i) outperformed the simplified approach ii) noticeably for $1/\sigma_e$ and slightly for κ. The hybrid model lowered by a factor 3 the relative standard deviation on thermal conductivity with respect to approach i).Similarly, correlating independently the electric and electronic thermal deviation functions produced the best fits from the hybrid model. Typically, reductions by a factor 2 and a factor 4 on the relative standard deviations on electric resistivity and thermal conductivity coefficients, respectively, were observed with respect to approach ii).

IV.3. Reduction of Electric/Thermal Conductivities in $Au_{1-c}Ag_c$ Alloy Nanoparticles

Simulations by the full model were attempted to assess the extent of deviations from bulk properties when electron-boundary and phonon-boundary scatterings come into play. Hence, reduction of electric and thermal conductivities described by Eqs. (15), (13), (25) contributions was sensed by means of the ratios κ_nanoparticle/κ_bulk and σ_e_nanoparticle/σ_e_bulk. The effects of particle sizes when they approach the mean free paths of the heat/current carriers and of impurity concentration were simulated under both electron-phonon equilibrium ($T_e = T_a$) and non-equilibrium ($T_e > T_a$). For a given particle size, when the electron gas is hotter than the lattice, the electronic thermal conductivity outpaces that where electron gas and lattice are in thermodynamic equilibrium. This can be assessed from Eq. (27) where the electron-phonon, and impurity and boundary scattering terms appear to diminish as T_e exceeds T_a.

The same cannot be said about electric conductivity. Its tendency is to be lower in non-equilibrium than in equilibrium because of the temperature independence of impurity and boundary scattering terms and of the T_e^2 decreasing trend (Eq. (26)). Figs. 4(a),(b) show the effect of particle size on κ_nanoparticle/κ_bulk and σ_e_nanoparticle/σ_e_bulk ratios under phonon-electron equilibrium ($T_e = T_a$) and non-equilibrium situations ($T_e > T_a$) for pure gold at various electron and phonon temperatures.

TABLE I
ANN CORRELATION FOR THE ELECTRIC DEVIATION FUNCTION Δ FROM MATHIESSEN'S ADDITIVITY RULE

$$\frac{\Delta(c,T)-\Delta_{exp}^{min}}{\Delta_{exp}^{max}-\Delta_{exp}^{min}} = \left(1+e^{-\sum_{j=1}^{j=6}\alpha_j H_j}\right)^{-1}$$

$$U_1 = \frac{c-c_{exp}^{min}}{c_{exp}^{max}-c_{exp}^{min}};\ U_2 = \frac{T_a-T_{exp}^{min}}{T_{exp}^{max}-T_{exp}^{min}};\ U_3 = 1;\ H_6 = 1$$

$$H_j = \left(1+e^{-\sum_{i=1}^{i=3}\alpha_{ij}U_i}\right)^{-1}$$

$\Delta_{exp}^{min} = -4.75\,10^{-9}$; $c_{exp}^{min} = 0.009092$; $T_{exp}^{min} = 200$; $\Delta_{exp}^{max} = 7.15\,10^{-9}$; $c_{exp}^{max} = 0.997256$; $T_{exp}^{max} = 1200$

		j=1	2	3	4	5
α_{ij}	i=1	34.3837	16.5346	-8.62987	-15.6637	-0.817441
	2	4.54326	6.55372	0.0336928	-6.3891	0.0796014
	3	-3.20786	-22.8086	2.92377	20.1288	2.39412
α_j	j=1	2	3	4	5	6
	-2.5789	43.2413	-7.37668	12.654	48.5589	-50.6035

As can be seen, reduction in gold electric and thermal conductivities is felt only when particle sizes fall below 1 μm.

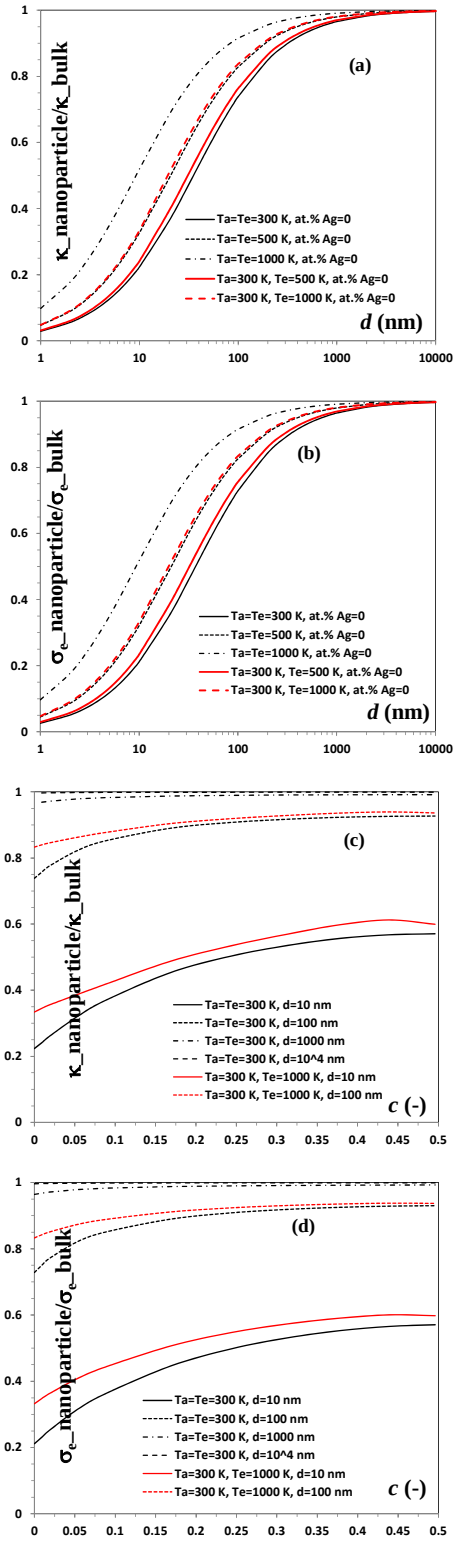

Figs. 4. Ratio of nanoparticle thermal and electric conductivities to bulk counterparts as a function of nanoparticle diameter (a,b) and solute concentration (c,d) assuming electron-phonon equilibrium and non-equilibrium at temperature from ambient to 1000 K for pure gold (a,b) and gold-silver alloys (c,d)

TABLE II

ANN CORRELATION FOR THE THERMAL DEVIATION FUNCTION δ FROM MATHIESSEN'S ADDITIVITY RULE

$$\frac{\delta(c,T)-\delta_{exp}^{min}}{\delta_{exp}^{max}-\delta_{exp}^{min}}=\left(1+e^{-\sum_{j=1}^{j=5}\beta_j H_j}\right)^{-1}$$

$$H_j=\left(1+e^{-\sum_{i=1}^{i=3}\beta_{ij}U_i}\right)^{-1}$$

$$U_1=\frac{c-c_{exp}^{min}}{c_{exp}^{max}-c_{exp}^{min}};\ U_2=\frac{T_a-T_{exp}^{min}}{T_{exp}^{max}-T_{exp}^{min}}$$

$$U_3=1;\ H_6=1$$

$\delta_{exp}^{min}=-6.5110^{-4}$; $c_{exp}^{min}=0.009092$; $T_{exp}^{min}=250$; $\delta_{exp}^{max}=5.09\,10^{-4}$; $c_{exp}^{max}=0.997256$; $T_{exp}^{max}=1200$

		j=1	2	3	4	5
β_{ij}	i=1	3.62616	21.9405	13.7364	-0.650004	7.7021
	2	0.709836	0.250993	0.471569	-7.52208	0.709105
	3	-0.17743	-0.946187	-2.81175	-3.05571	-1.34693
β_j	j=1	2	3	4	5	6
	-50.2173	-8.80694	-21.034	-31.5593	65.4455	14.0296

TABLE III

STATISTICAL FIGURES OF MERIT OF THREE APPROACHES FOR ESTIMATING ELECTRIC AND THERMAL CONDUCTIVITIES FOR $Au_{1-C}Ag_C$ ALLOY SYSTEMS*

	SDR (%)	SDA (Ω.m; W/m/K)	AARE (-)	AAE (Ω.m; W/m/K)
Full model	σ 1.6	$1.3\ 10^{-9}$	0.6	$0.5\ 10^{-9}$
	κ 0.7	1.9	0.5	1.1
approach i)	σ 1.6	$1.3\ 10^{-9}$	0.6	$0.5\ 10^{-9}$
$\delta=\Delta/(L_0T)$	κ 2.1	5.9	1.6	3.5
approach ii)	σ 3.1	$2.7\ 10^{-9}$	2.7	$2.3\ 10^{-9}$
$\Delta=0$, $\delta=0$	κ 2.9	5.1	2.8	4.7

*SDR = standard deviation on relative residuals; SDA = standard deviation on absolute residuals; AARE = average absolute relative error; AAE = average absolute error

It is worth noting that similar trends and size threshold were predicted from a simpler thermal conductivity model proposed by Hopkins et al. [15] to account for boundary scattering in gold nanowires under equilibrium and non-equilibrium. These trends were coherent with those reported Xia et al. [7] for the correlation of thermal and electric conductivities for nano-porous gold foils.

Also, predicted trends from the electric conductivity model, Eq. (26), as a function of size qualitatively adheres to the findings from Ma et al. [8] on electric resistivity determinations for polycrystalline thin gold films.

The increased tendency of the thermal conductivity ratio as a function of temperature is due both to lattice and electron gas temperatures as can be appreciated from their impact on the conductivity ratio in equilibrium and non-equilibrium (Fig. 4(a)). The electric resistivity ratio behaves qualitatively in a similar manner with a tendency for this ratio to grow as temperature increases thus reducing the gap between bulk and nanometric transport properties (Fig. 4(b)). The increased concentration of silver solute in the gold-silver solution also has a tendency to increase both thermal (Fig. 4(c)) and electric (Fig. 4(d)) conductivity ratios with a more pronounced impact for the smaller nanoparticles. Also, hotter electrons in non-equilibrium have the tendency to further narrow the deviation between bulk and nanometric transport properties.

V. Conclusion

State of the art methods were revisited for the estimation of electric and thermal transport coefficients in gold-silver alloys with emphasis on the temperature

range above the metals Debye temperatures. The dominant scattering mechanisms affecting electric and thermal conductivities in gold-silver alloys were accounted for while embracing specimen dimensions extending from bulk to nanometric scale and by considering both electron-phonon equilibrium and non-equilibrium situations.

Two artificial neural network correlations as a function of silver atom fraction and temperature were developed to account for the deviations of electric and electronic thermal transport vis-à-vis Matthiessen's additivity rule of the dominant scattering mechanisms in the gold-silver solutions. The hybrid approach thus developed was confronted and validated against a large repository of data recommended by CINDAS (Center for Information and Numerical Data Analysis and Synthesis) for the electric and thermal conductivity properties of gold-silver alloy systems encompassing pure metals and full binary-solution composition range.

References

[1] J. Marsden, I. House, *The chemistry of gold extraction*, Ellis Horwood Series in Metals and Associated Materials: Great Britain, (1992).

[2] A. Azizi, C.F. Petre, C. Olsen, F. Larachi, Untangling galvanic and passivation phenomena induced by sulfide minerals on precious metal leaching using a new packed-bed electrochemical cyanidation reactor, *Hydrometallurgy* 107 *(2011) 101-111.*

[3] Y. Zhang, R.W. Cattrall, I.D. McKelvie, S.D. Kolver, Gold, an alternative to platinum group metals in automobile catalytic converters, *Gold Bull.* 44 *(2011) 145-153*.

[4] C.W. Corti, R.J. Holliday, Commercial aspects of gold applications: From materials science to chemical science, *Gold Bull.* 37 *(2004) 20-26.*

[5] C. Burda, X. Chen, R. Narayanan, M.A. ElSayed, Chemistry and properties of nanocrystals of different shapes, *Chem. Rev.* 105 *(2005) 1025-1102.*

[6] L. Polavarapu, Q.H. Xu, A simple method for large scale synthesis of highly monodisperse gold nanoparticles at room temperature and their electron relaxation properties, *Nanotechnology* 20 *(2009) 185606.*

[7] R. Xia, J.L. Wang, R. Wang, X. Li, X. Zhang, X.Q. Feng, Y. Ding, Correlation of the thermal and electrical conductivities of nanoporous gold, *Nanotechnology* 21 *(2010) 085703.*

[8] W.G. Ma, H.D. Wang, X. Zhang, W. Wang, Experiment study of the size effects on electron-phonon relaxation and electrical resistivity of polycrystalline thin gold films, *J. Appl. Phys.* 108 *(2010) 0643087.*

[9] J. Wang, R. Xia, J. Zhu, Y. Ding, X. Zhang, Y. Chen, Effect of thermal coarsening on the thermal conductivity of nanoporous gold, *J. Mat. Sci.* 47 *(2012) 5013-5018.*

[10] P.G. Klemens, R.K. Williams, Thermal conductivity of metals and alloys, *Int. Metals Rev.* 31 (1986) 197-215.

[11] C.Uher, Thermal conductivity of metals. In: Tritt TM (ed.) *Thermal conductivity-Theory, properties and applications*, Kluwer Academic/Plenum Publishers, New York, pp 21-91, 2004.

[12] C.Y. Ho, M.W. Ackerman, K.Y. Wu, S.G. Oh, T.N. Havill, Thermal conductivity of ten selected binary alloy systems, *J. Phys. Chem. Ref. Data* 7 (1978) 959-1177.

[13] C.Y. Ho, M.W. Ackerman, K.Y Wu, T.N. Havill, R.H. Bogaard, R.A. Matula, S.G Oh, H.M. James, Electrical resistivity of ten selected binary alloy systems, *J. Phys. Chem. Ref. Data* 12 *(1983) 183-322.*

[14] D.S. Ivanov, L.V. Zhigilei, Combined atomistic-continuum modeling of short-pulse laser melting and disintegration of metal films, *Phys. Rev. B* 68 (2003) 064114.

[15] P.E. Hopkins, P.M. Norris, L.M. Phinney, S.A. Policastro, R.G. Kelly, Thermal conductivity in nanoporous gold films during electron-phonon non-equilibrium, *J. Nanomaterials (2008) doi:10.1155/2008/418050.*

[16] P.E. Hopkins, J.L. Kassebaum, P.M. Norris, Effects of electron scattering at metal-nonmetal interfaces on electron-phonon equilibration in gold films, *J. Appl. Phys.* 105 *(2009) 023710.*

[17] J. Yang, Theory of thermal conductivity. In: Tritt TM (ed.) *Thermal conductivity-Theory, properties and applications*, Kluwer Academic/Plenum Publishers, New York, pp 1-20 (2004).

[18] J.E. Graebner, M.E. Reiss, L. Seibles, T.M. Hartnett, R.P. Miller, C.J. Robinson, Phonon scattering in chemical-vapor-deposition diamond, *Phys. Rev. B* 50 *(1994) 3702-3713.*

[19] N.W. Ashcroft, N.D. Mermin, *Physique des solides*. Transl. F. Biet and H. Kachkachi, EDP Sciences, France (2002).

[20] J.C. Kraut, W.B. Stern, The density of gold-silver-copper alloys and its calculation from the chemical composition, *Gold Bull.* 33 *(2000) 52-55.*

[21] G.A. Slack, S. Galginaitis, Thermal conductivity and phonon scattering by magnetic impurities in CdTe, *Phys. Rev.* 133 *(1964) A253-A268.*

[22] N.V. Novikov, A.P. Podoba, S.V. Shmegera, A. Witek, A.M. Zaitsev, A.B. Denisenko, W.R. Fahrner, M. Werner, Influence of isotopic content on diamond thermal conductivity, *Diamond & Related Materials* 8 (1999) 1602-1606.

[23] R.E.B. Makinson, The thermal conductivity of metals, *Proc. Camb. Phil. Soc.* 34 *(1938) 474-497.*

[24] C.Y. Ho, R.W. Powell, P.E. Liley, Thermal conductivity of the elements. *J. Phys. Chem. Ref. Data* 1 *(1972) 279-421.*

[25] P. Cloutier, C. Tibirna, B.P.A. Grandjean, J. Thibault, NNfit, logiciel de régression utilisant les réseaux à couches, http://www.ulaval.ca/~nnfit, Laval university, Canada (1996).

[26] F. Larachi, L. Belfares, I. Iliuta, B.P.A Grandjean, Heat and mass transfer in cocurrent gas-liquid packed beds: Analysis, recommendations, and new correlations, *Ind. Eng. Chem. Res.* 42 *(2003) 222-242.*

[27] M. Kaveh, N. Wiser, Electron-electron scattering in conducting materials. Adv. Phys. 33 *(1984) 257-372.*

Authors' information

Caroline Olsen holds a B.Sc. and M.Sc. in Chemistry from University of Sherbrooke (Québec-Canada). She is in charge at COREM of the cyanidation and flotation teams of the mining industry operations. COREM Research Center - 1180, rue de la Minéralogie, Québec City, QC, Canada G1N 1X7.
E-mail: caroline.olsen@corem.qc.ca

Faïçal Larachi (Corresponding author) is full professor of chemical engineering. He holds a doctoral degree from the Institut National Polytechnique de Lorraine in France. His research interests encompass multiphase reactor engineering, mineral processing and new approaches for mitigation of greenhouse gas effect. Department of chemical engineering, Laval University, Quebec, QC, G1V 0A6, Canada and COREM Research Center - 1180, rue de la Minéralogie, Québec City, QC, Canada G1N 1X7.
Tel: 1-418-656-3566
Fax: 1-418-656-5993
E-mail: faical.larachi@gch.ulaval.ca